Mid-infrared nonlinear optical response of Si-Ge waveguides with ultra-short optical pulses

L. Carletti,[1,5] M. Sinobad,[4] P. Ma,[2] Y. Yu,[2] D. Allioux,[1] R. Orobtchouk,[1] M. Brun,[3] S. Ortiz,[3] P. Labeye,[3] J. M. Hartmann,[3] S. Nicoletti,[3] S. Madden,[2] B. Luther-Davies,[2] D. J. Moss,[4] C. Monat,[1] and C. Grillet[1,6]

[1]*University of Lyon, Institut des Nanotechnologies de Lyon, Ecole Centrale de Lyon, Ecully, France*
[2] *CUDOS, Laser Physics Centre, Australian National University, Canberra, ACT 0100 Australia*
[3] *CEA-LETI MINATEC Campus, Grenoble, France*
[4]*School of Electrical and Computer Engineering, RMIT University, Melbuorne, VIC 3001, Australia*
[5]*luca.carletti@unibs.it*
[6]*christian.grillet@ec-lyon.fr*

Abstract: We characterize the nonlinear optical response of low loss $Si_{0.6}Ge_{0.4}$ / Si waveguides in the mid-infrared between 3.3 μm and 4 μm using femtosecond optical pulses. We estimate the three and four-photon absorption coefficients as well as the Kerr nonlinear refractive index from the experimental measurements. The effect of multiphoton absorption on the optical nonlinear Kerr response is evaluated and the nonlinear figure of merit estimated providing some guidelines for designing nonlinear optical devices in the mid-IR. Finally, we compare the impact of free-carrier absorption at mid-infrared wavelengths versus near-infrared wavelengths for these ultra-short pulses.

OCIS codes: (190.4390) Nonlinear optics, integrated optics; (190.4400) Nonlinear optics, materials; (230.3120) Integrated optics devices; (130.2790) Guided waves; (130.3060) Infrared.

References and links

1. R. Soref, "Mid-infrared photonics in silicon and germanium," Nat. Photonics **4**(8), 495–497 (2010).
2. B. Jalali, "Nonlinear optics in the mid-infrared," Nat. Photonics **4**(8), 506–508 (2010).
3. F. K. Tittel, D. Richter, and A. Fried, "Mid-Infrared Laser Applications in Spectroscopy," in Solid-State Mid-Infrared Laser Sources, (Springer Berlin Heidelberg, 2003).
4. http://www.mirifisens-project.eu/, "Mid infrared innovative lasers for improved sensor of hazardous substances
5. http://optics.org/news/6/2/23, "mirSense integrated QCLs target gas-sensing and biomed roles.".
6. G. C. M.Carras, G. Maisons, B. Simozrag, V. Trinite, M. Brun, S. Nicoletti, L.Orbe, "Advances toward monolithic broadly-tunable QCL sources," in Proc. SPIE 8993 (INVITED) Quantum Sensing and Nanophotonic Devices XI, 2014.
7. M. C. L. J. Orbe, G . Carpintero, G. Maisons, C. Gilles, F. Boulila, "MIR Photonic Integrated Circuits for Laser Spectroscopy," in MIOMD - Mid-IR Optoelectronics : Materials and Devices (2014).
8. B. Kuyken, X. Liu, R. M. Osgood, Jr., R. Baets, G. Roelkens, and W. M. J. Green, "Mid-infrared to telecom-band supercontinuum generation in highly nonlinear silicon-on-insulator wire waveguides," Opt. Express **19**(21), 20172–20181 (2011).
9. N. Singh, D. D. Hudson, Y. Yu, C. Grillet, S. D. Jackson, A. Casas-Bedoya, A. Read, P. Atanackovic, S. G. Duvall, S. Palombo, D. J. Moss, B. Luther-Davies, and B. J. Eggleton, "Mid-IR supercontinuum generation from 2-6 um in a silicon nanowire," Optica **2**(9), 797–802 (2015).
10. M. A. Ettabib, L. Xu, A. Bogris, A. Kapsalis, M. Belal, E. Lorent, P. Labeye, S. Nicoletti, K. Hammani, D. Syvridis, D. P. Shepherd, J. H. V. Price, D. J. Richardson, and P. Petropoulos, "Broadband telecom to mid-infrared supercontinuum generation in a dispersion-engineered silicon germanium waveguide," Opt. Lett. **40**(17), 4118–4121 (2015).
11. B. Kuyken, T. Ideguchi, S. Holzner, M. Yan, T. W. Hänsch, J. Van Campenhout, P. Verheyen, S. Coen, F. Leo, R. Baets, G. Roelkens, and N. Picqué, "An octave-spanning mid-infrared frequency comb generated in a silicon nanophotonic wire waveguide," Nat. Commun. **6**, 6310 (2015).
12. A. G. Griffith, R. K. W. Lau, J. Cardenas, Y. Okawachi, A. Mohanty, R. Fain, Y. H. D. Lee, M. Yu, C. T. Phare, C. B. Poitras, A. L. Gaeta, and M. Lipson, "Silicon-chip mid-infrared frequency comb generation," Nat. Commun. **6**, 6299 (2015).

#249304 Received 7 Sep 2015; revised 23 Oct 2015; accepted 25 Oct 2015; published 4 Dec 2015

13. S. Zlatanovic, J. S. Park, S. Moro, J. M. C. Boggio, I. B. Divliansky, N. Alic, S. Mookherjea, and S. Radic, "Mid-infrared wavelength conversion in silicon waveguides using ultracompact telecom-band-derived pump source," Nat. Photonics **4**(8), 561–564 (2010).
14. X. Liu, R. M. Osgood, Jr., Y. A. Vlasov, and W. M. J. Green, "Mid-infrared optical parametric amplifier using silicon nanophotonic waveguides," Nat. Photonics **4**(8), 557–560 (2010).
15. J. Leuthold, C. Koos, and W. Freude, "Nonlinear silicon photonics," Nat. Photonics **4**(8), 535–544 (2010).
16. C. Grillet, L. Carletti, C. Monat, P. Grosse, B. Ben Bakir, S. Menezo, J. M. Fedeli, and D. J. Moss, "Amorphous silicon nanowires combining high nonlinearity, FOM and optical stability," Opt. Express **20**(20), 22609–22615 (2012).
17. B. Corcoran, C. Monat, C. Grillet, D. J. Moss, B. J. Eggleton, T. P. White, L. O. Faolain, and T. F. Krauss, "Green light emission in silicon through slow-light enhanced third-harmonic generation in photonic- crystal waveguides," Nat. Photonics **3**(4), 206–210 (2009).
18. X. Gai, Y. Yu, B. Kuyken, P. Ma, S. J. Madden, J. Van Campenhout, P. Verheyen, and R. Baets, "Nonlinear absorption and refraction in crystalline silicon in the mid-infrared," Laser Photonics Rev. **7**(6), 1–11 (2013).
19. T. Wang, N. Venkatram, J. Gosciniak, Y. Cui, G. Qian, W. Ji, and D. T. H. Tan, "Multi-photon absorption and third-order nonlinearity in silicon at mid-infrared wavelengths," Opt. Express **21**(26), 32192–32198 (2013).
20. N. K. Hon, R. Soref, and B. Jalali, "The third-order nonlinear optical coefficients of Si, Ge, and Si1−xGex in the midwave and longwave infrared," J. Appl. Phys. **110**(1), 011301 (2011).
21. M. Brun, P. Labeye, G. Grand, J. M. Hartmann, F. Boulila, M. Carras, and S. Nicoletti, "Low loss SiGe graded index waveguides for mid-IR applications," Opt. Express **22**(1), 508–518 (2014).
22. L. Carletti, P. Ma, Y. Yu, B. Luther-Davies, D. Hudson, C. Monat, R. Orobtchouk, S. Madden, D. J. Moss, M. Brun, S. Ortiz, P. Labeye, S. Nicoletti, and C. Grillet, "Nonlinear optical response of low loss silicon germanium waveguides in the mid-infrared," Opt. Express **23**(7), 8261–8271 (2015).
23. K. Hammani, M. A. Ettabib, A. Bogris, A. Kapsalis, D. Syvridis, M. Brun, P. Labeye, S. Nicoletti, D. J. Richardson, and P. Petropoulos, "Optical properties of silicon germanium waveguides at telecommunication wavelengths," Opt. Express **21**(14), 16690–16701 (2013).
24. K. Hammani, M. A. Ettabib, A. Bogris, A. Kapsalis, D. Syvridis, M. Brun, P. Labeye, S. Nicoletti, and P. Petropoulos, "Towards nonlinear conversion from mid- to near-infrared wavelengths using Silicon Germanium waveguides," Opt. Express **22**(8), 9667–9674 (2014).
25. G. P. Agrawal, Nonlinear Fiber Optics. (Academic Press, 2001).
26. P. Ma, D. Y. Choi, Y. Yu, X. Gai, Z. Yang, S. Debbarma, S. Madden, and B. Luther-Davies, "Low-loss chalcogenide waveguides for chemical sensing in the mid-infrared," Opt. Express **21**(24), 29927–29937 (2013).
27. I. W. Hsieh, X. Chen, J. I. Dadap, N. C. Panoiu, R. M. Osgood, S. J. McNab, and Y. A. Vlasov, "Ultrafast-pulse self-phase modulation and third-order dispersion in Si photonic wire-waveguides," Opt. Express **14**(25), 12380–12387 (2006).
28. S. Combrie, Q. V. Tran, A. De Rossi, C. Husko, and P. Colman, "High quality GaInP nonlinear photonic crystals with minimized nonlinear absorption," Appl. Phys. Lett. **95**(22), 221108 (2009).
29. Q. Lin, O. J. Painter, and G. P. Agrawal, "Nonlinear optical phenomena in silicon waveguides: modeling and applications," Opt. Express **15**(25), 16604–16644 (2007).

1. Introduction

The mid-infrared (mid-IR) region of the spectrum, at wavelengths between 3 μm and 20 μm, is currently gaining formidable momentum since it is particularly rich in applications that can potentially impact many important aspects of our everyday life such as chemical and biological sensing, active imaging, tissue ablation, secure free-space communication, multi-wavelength light sources, and many others [1,2]. Molecular sensing devices with unprecedented sensitivity, exploiting the strong fundamental rotational-vibrational absorption lines that many molecules exhibit in the mid-IR [3], are currently being developed and are in the process of commercialisation [4,5]. However, despite the tremendous recent progress in miniaturisation, reduced power consumption, and increased tunability of detection and spectroscopy platforms developed thus far for the mid-IR [6,7], current technologies are still primarily based on stand-alone single frequency laser sources that operate in relatively narrow spectral regions. This limits the number of different molecules that can be detected with a single system. An appealing approach that has been suggested by the silicon photonics community is to create mid-IR CMOS compatible integrated photonic platforms [1,2] that are capable of yielding broadband optical sources via nonlinear effects such as supercontinuum, frequency combs, and others [8–14]. More generally, the mid-IR has been predicted to be a promising wavelength range for nonlinear devices based on group IV materials (like Si, Ge and Si-Ge). In particular, the nonlinear loss associated with two photon absorption (TPA) that limits device performance in all of these materials at telecom wavelengths [15–17] vanishes at

#249304 Received 7 Sep 2015; revised 23 Oct 2015; accepted 25 Oct 2015; published 4 Dec 2015

longer wavelengths. This potentially could open the door to realizing photonic devices with new capabilities such as, super continuum [8–10], wide bandwidth frequency combs [11,12] and parametric waveguide amplifiers with positive net gain [13,14]. However, apart from one report of nonlinear optics out to 6 μm in the silicon on sapphire (SOS) platform [9], Si has hardly been investigated beyond the short-wavelength infrared (SWIR), limited to 3 μm, due to both absorption in the cladding material (i.e. silica in the case of the silicon on insulator (SOI)) and the impact of higher order (3 and 4) photon absorption and the ensuing free carrier absorption [18,19].

For mid-IR applications, Si-Ge alloys on Si are an emerging attractive alternative platform to SOI [1,20]. The wide transparency window of this material as well as significant progress on deposition and fabrication techniques have enabled some very promising results in both linear [21,22] and nonlinear performance [10,22–24] in the last year alone. Ridge waveguides in $Si_{0.6}Ge_{0.4}$/Si with a graded refractive index distribution in the core that were designed for low loss operation over the entire 3 μm to 8 μm wavelength region have been reported [21]. The scattering loss could be minimized because of the use of a graded index structure (which also limits potential misfit dislocations between the cladding Si and core Si-Ge) and this resulted in linear propagation losses as low as 1 dB/cm at $\lambda = 4.5$ μm and 2 dB/cm at $\lambda = 7.4$ μm. Further, step index $Si_{0.6}Ge_{0.4}$/Si waveguides, with typical cross sections of 1.4×2 μm^2, were shown in [22] to be a viable platform with propagation losses at $\lambda = 4.75$ μm of around 0.5 dB/cm due in part to the very low density of core/cladding interface defects. Very recently, demonstrations of four wave mixing in Si-Ge have been shown in the near-IR [23] and in the SWIR out to a wavelength of 2.6 μm [24]. Further, the first demonstration of supercontinuum generation between 1.5 μm and 2.8 μm in Si-Ge has been achieved [10]. In early 2015, the first experimental investigation of the nonlinear optical response of step index Si-Ge/Si waveguides in the actual mid-IR range (from 3.25 μm up to 4.75 μm) was reported by measuring self-phase modulation (SPM) of picosecond optical pulses [22]. Three and four-photon absorption coefficients, as well as the Kerr nonlinear refractive index, were found to be of the same order of magnitude as those in crystalline Si.

Here, we report experimental measurements of the nonlinear optical response of step index Si-Ge/Si waveguides in the mid-IR obtained by measuring self-phase modulation (SPM) and the nonlinear transmission of these waveguides at high optical intensities (exceeding 100 GW/cm^2) using femtosecond optical pulses at wavelengths between 3.3 μm and 4 μm. In contrast with [22], where picosecond long pulses were used, the use of femtosecond pulses reduces the impact of free-carriers on the device performance. Furthermore, we investigate several different waveguide geometries and lengths in order to increase the accuracy of our findings. Our results are in agreement with [22], corroborating our previously estimated values of the nonlinear parameters. Using our results, we evaluate the nonlinear figure of merit (FOM) and we observe an optimum around wavelengths of 4 μm that is due to the decrease of the three-photon absorption coefficient, together with a small four-photon absorption coefficient. We find that this optimum of the FOM also depends on the coupled peak intensity since the three and four-photon absorption scale differently with this parameter. We observe that the impact of free-carriers is significant even though the pulse duration is only a few hundreds of femtoseconds, in contrast with what is usually observed at near-IR wavelengths, and highlights the need to accurately account for free-carrier effects even when using ultra-short optical pulses in the mid-IR. The results presented here significantly expand the parameter space investigated for the nonlinear optical response of this material platform, thus providing an important foundation for designing nonlinear devices for this wavelength range. Finally, in order to illustrate this, we report calculations demonstrating the feasibility of designing efficient mid-IR supercontinuum source based on Si-Ge/Si waveguides.

#249304 Received 7 Sep 2015; revised 23 Oct 2015; accepted 25 Oct 2015; published 4 Dec 2015

2. Device fabrication and experiment

An example of one of the devices under test is shown in Fig. 1. They consist of step-index ridge waveguides with a $Si_{0.6}Ge_{0.4}$ core grown on a Si substrate and encapsulated in a Si cladding. Both core and cladding materials are in crystalline form. The refractive index difference between Si and $Si_{0.6}Ge_{0.4}$ in the wavelength range used in these experiments is about 0.17. This percentage of Ge was chosen because it allowed us to increase the material optical nonlinear response while tempering the lattice mismatch between the Si-Ge core and the Si cladding thus minimizing crystalline stress. This enabled the fabrication of high quality low defects structures necessary for obtaining low loss devices. Two 200 mm Si wafers were processed (fabrication details are given in [22]); the thickness of the deposited $Si_{0.6}Ge_{0.4}$ layer was 2.7 μm for the first wafer and 1.4 μm for the second.

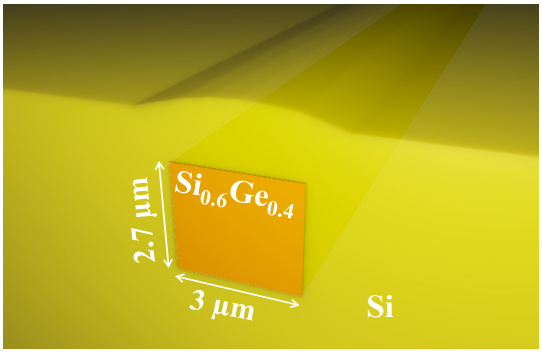

Fig. 1. Schematic representation of one of the ridge waveguides. The color orange represent the $Si_{0.6}Ge_{0.4}$ core that is surrounded by crystalline Si (in yellow).

Table 1. Geometrical properties of the waveguides and mode properties extracted from simulations at the wavelengths used in the experiment.

	waveguide 1		*waveguide 2*
Height (μm) × Width (μm)	3 × 2.7		2 × 1.4
Length (cm)	3		5.7
Wavelength (μm)	3.3	3.75	4
β_2 (ps^2/m)	0.96	1.16	1.52
β_3 (ps^3/m)	-2×10^{-3}	2.8×10^{-3}	-7.1×10^{-3}
β_4 (ps^4/m)	2.7×10^{-5}	1.8×10^{-3}	5.3×10^{-3}
A_{3eff} (μm^2)	6.9	7.7	6.8
A_{5eff} (μm^2)	6.1	6.7	5.6
A_{7eff} (μm^2)	5.6	6.2	5

Waveguides were fabricated in order to measure the nonlinear optical response of $Si_{0.6}Ge_{0.4}$, and had a cross-section of 3 × 2.7 μm^2 and a length of 3 cm for the first wafer (*waveguide 1*) and a cross-section of 2 × 1.4 μm^2 and a length of 6 cm on the second wafer (*waveguide 2*). The mode properties, such as dispersion and mode effective area, were calculated from finite element method simulations (FEMSIM), and are shown in Table 1. The calculations were performed by including the material dispersion of Si [15] and $Si_{0.6}Ge_{0.4}$ (measured at CEA-LETI) in the wavelength range used in our experiments. The effective mode area [25] was around 7 μm^2 for both waveguides. The waveguide dispersion was not engineered and thus the group velocity dispersion (GVD) was normal for both waveguides with a β_2 parameter between + 0.96 ps^2/m and + 1.5 ps^2/m in the wavelength range of the experiment. Hence, for a 320 fs long optical pulse, the dispersion length was between 1.9 cm and 1.2 cm, which is shorter than the waveguides used in these experiments.

#249304 Received 7 Sep 2015; revised 23 Oct 2015; accepted 25 Oct 2015; published 4 Dec 2015

The transmission measurements were performed using a tunable optical parametric amplifier (OPA) that emitted near transform-limited Gaussian pulses with a full-width at half maximum (FWHM) duration of 320 fs at 21 MHz repetition rate and at wavelengths between 3 µm and 4 µm. The setup was otherwise similar to that used in [22]. The transmitted power was measured with a PbSe detector combined with lock-in detection [26]. The transmitted spectrum was measured with a Newport Cornerstone 260 1/4m monochromator with a 150 l/mm grating.

3. Results

The nonlinear optical response of the Si-Ge/Si waveguides was analyzed from nonlinear transmission and SPM measurements, with increasing input peak powers using femtosecond optical pulses at 3.3 µm and 3.75 µm for waveguide 1 and at 4 µm for waveguide 2. A selection of the measured output spectra are shown in Figs. 2(a), 2(c), and 2(e) and the complete set of measurements on the 2D maps of Figs. 2(b), 2(d), and 2(f). The characteristic side lobes of the SPM phenomenon are reduced due to the effects of dispersion, which, as mentioned above, is not negligible for 320 fs long pulses. The broadening exhibited by the measured spectra initially increases rapidly with increasing coupled peak intensity, and then tends to roll-off. This observation is confirmed in Fig. 3(a), which displays the normalized RMS spectral broadening extracted from the measured spectra as a function of the coupled peak intensity. These curves clearly are a sub-linear function of the coupled peak intensity, which might indicate the presence of nonlinear losses [25].

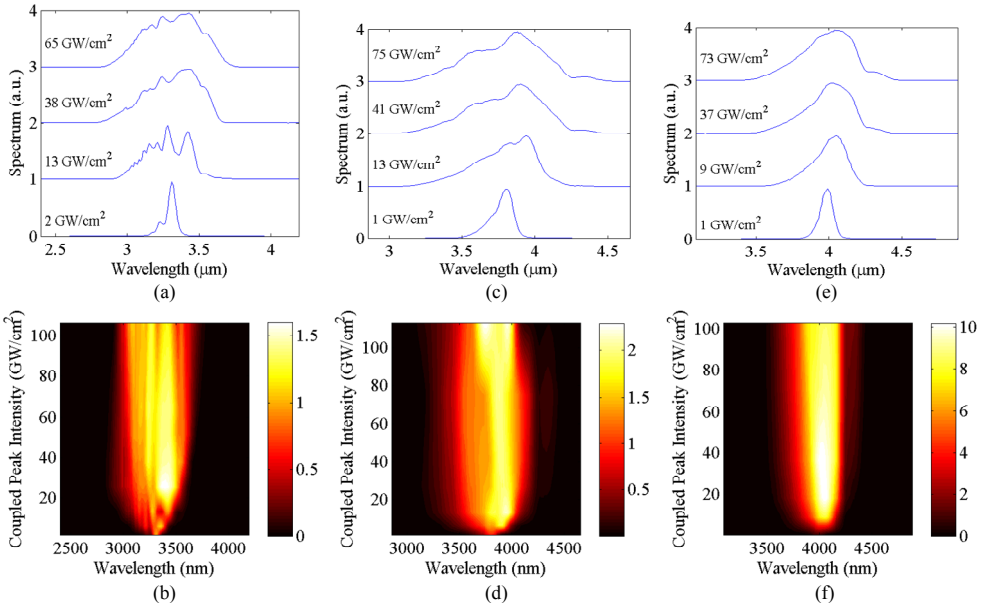

Fig. 2. Normalized transmitted spectrum as a function of the coupled peak intensity for femtosecond pulses centered at wavelengths of 3.3 µm (a), (b) 3.75 µm (c), (d) and 4 µm (e), (f). Spectra (a), (b), (c) and (d) are measured using *waveguide 1* whereas spectrum (e) and (f) is measured using *waveguide 2*.

In order to obtain the multi-photon absorption coefficients of the $Si_{0.6}Ge_{0.4}$/Si waveguides, the average output power was measured as a function of the coupled peak intensity, the results of which are shown in Fig. 3(b). The measured output power increased almost linearly with the input power at low intensities until it saturated above ~20 GW/cm^2, clearly confirming the presence of nonlinear losses in the waveguide. The trend observed in Fig. 3(b) is similar to optical limiting arising from TPA in the near-infrared region for using femtosecond pulses

#249304 Received 7 Sep 2015; revised 23 Oct 2015; accepted 25 Oct 2015; published 4 Dec 2015

[27]. Since the wavelength range of our experiments is significantly longer than the TPA threshold of $Si_{0.6}Ge_{0.4}$ (i.e. $\lambda_{th} \approx 2.45$ μm [20]), the nonlinear absorption observed in Fig. 3(b) is necessarily due to higher order multi-photon absorption, such as three- or four-photon absorption [18,22].

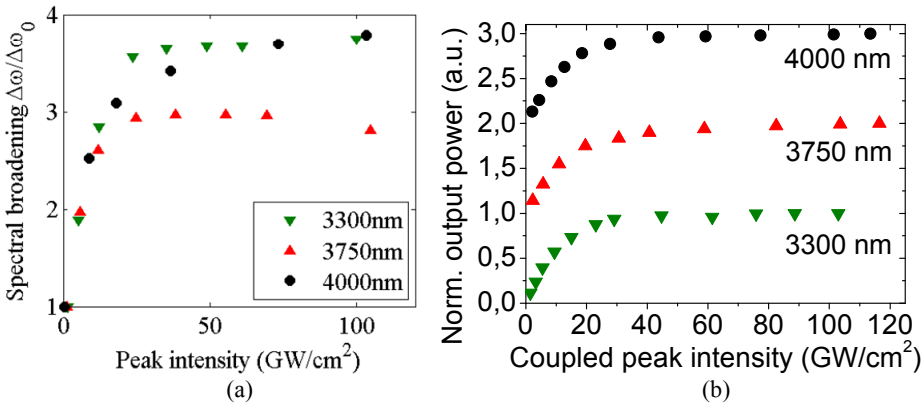

Fig. 3. (a) Spectral broadening as a function the coupled peak intensity. (b) Normalized transmitted power as a function of the coupled peak intensity measured using pulses centered at 3300 nm (downwards green triangles) and 3750 nm (upwards red triangles) from *waveguide 1* and at 4000 nm from *waveguide 2* (black dots). The two curves at 3750nm and 4000nm have been shifted vertically for clarity.

4. Analysis and discussion

In order to estimate the N-photon absorption coefficients, the linear relations between $1/T^N$ and the P_0^N, where T is the transmission and P_0 is the coupled peak power, are generally used (e.g [16, 28].). However, since the effect of dispersion is not negligible in our experiment, this approach could not be applied. Furthermore, the dephasing induced by the Kerr effect and by free-carrier induced dispersion influences the total transmitted power through the waveguide. Therefore, it is necessary to solve the nonlinear Schrödinger equation (NLSE) by including the Kerr effect as well as, three- and four-photon absorption, and free-carrier effects [22]. This yields:

$$\frac{\partial A}{\partial z}+\frac{\mathrm{i}}{2}\beta_2\frac{\partial^2 A}{\partial t^2}-\frac{i}{6}\beta_3\frac{\partial^3 A}{\partial t^3}+\frac{\mathrm{i}}{24}\beta_4\frac{\partial^4 A}{\partial t^4}+\frac{\alpha}{2}A= \\ \mathrm{i}\frac{k_0 n_2}{\mathrm{A}_{3\mathrm{eff}}}|A|^2 A-\frac{\alpha_{3PA}}{2\mathrm{A}_{5\mathrm{eff}}^2}|A|^4 A-\frac{\alpha_{4PA}}{2\mathrm{A}_{7\mathrm{eff}}^3}|A|^6 A-\frac{\sigma}{2}(1-\mathrm{i}\mu)N_c A \tag{1}$$

where A is the slowly varying envelope of the pulse electric field amplitude, β_2 is the second-order dispersion, β_3 is the third-order dispersion, β_4 is the fourth-order dispersion, α is the linear loss parameter, k_0 is the wavenumber, n_2 is the nonlinear refractive index, α_{3PA} and α_{4PA} are the three and four-photon absorption coefficients, A_{3eff}, A_{5eff} and A_{7eff} are the effective mode areas related to the nonlinear phenomena of different orders [22], σ is the free-carrier absorption parameter, and $\mu = 2k_c k_0/\sigma$ with k_c the free-carrier dispersion parameter. The rate equation governing the related free-carrier density, N_c, generated by three- and four-photon absorption is given by

$$\frac{\partial N_c}{\partial t}=\frac{\alpha_{3PA}}{3\hbar\omega}\left(\frac{|\mathrm{A}|^2}{A_{5eff}}\right)^3+\frac{\alpha_{4PA}}{4\hbar\omega}\left(\frac{|\mathrm{A}|^2}{A_{7eff}}\right)^4-\frac{N_c}{\tau_c} \tag{2}$$

#249304 Received 7 Sep 2015; revised 23 Oct 2015; accepted 25 Oct 2015; published 4 Dec 2015

where $\hbar$ is the reduced Plank constant, ω is the central angular frequency of the input pulse, and τ_c is the free-carrier lifetime. Since the range of values for τ_c reported for integrated waveguides is much longer than our pulse duration and shorter than the time period between two subsequent pulses, the last term on the right hand side of Eq. (2) was neglected [15]. As a starting point, the values for the free-carrier absorption and dispersion parameters of silicon were used and the scaling rules for the wavelength used in [18, 22] were applied giving $\sigma(\lambda) = 1.45 \times 10^{-21} \times (\lambda/1.55)^2$ m^2 and $k_c(\lambda) = 1.35 \times 10^{-27} \times (\lambda/1.55)^2$ m^3, where λ is the wavelength (in μm).

The NLSE in Eq. (1) was solved numerically using the Split-Step Fourier Method. In order to estimate the N-photon absorption coefficient α_{NPA} and the nonlinear refractive index n_2 for a given wavelength, an iterative method was adopted. In the first step, α_{NPA} was estimated by fitting the experimental transmission in Fig. 3(b) using Eqs. (1) and (2). In this first iteration, the n_2 value used was taken from [22]. In the second step, the value of α_{NPA} from the previous step was used to estimate n_2 by numerically reproducing the SPM spectra shown in Fig. 2. At this point, if the new estimated n_2 was different from the one that was used in the first step, then α_{NPA} was estimated again by using the latest value of n_2. The two steps were repeated until the values of α_{NPA} and n_2 converged. As it can be seen from Fig. 4(a), good agreement was found between the simulations and experiments for the normalized nonlinear transmission (defined as $T_{NL} = P_{out}/[P_{in} \times \exp(-\alpha L)]$, where P_{out} and P_{in} are the output and input peak powers, and L is the waveguide length) as a function of the coupled peak intensity. An example of the transmission spectra calculated using Eqs. (1) and (2) is shown in Fig. 4(b) and 4(c). The waveguide used for the calculation was *waveguide 2* and the input pulse was centered at 4 μm. As it can be seen in Fig. 4(c), these results reproduced the measurements shown in Fig. 2(e) relatively well. Good agreement between the simulations and experiments was also found for the normalized RMS spectral broadening extracted from the spectra of the transmitted pulse (see Fig. 4(d)). These results reproduced the measurements shown in Fig. 2(e) relatively well.

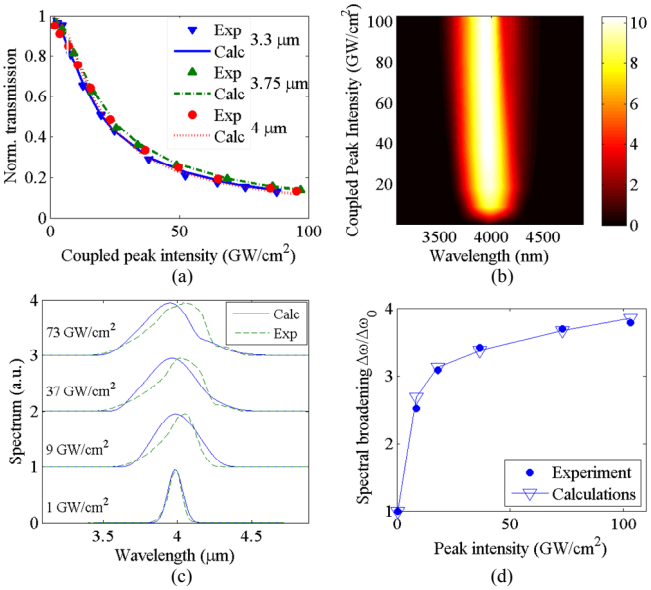

Fig. 4. (a) Numerical calculation (Calc) of the transmission as a function of wavelength compared to experiment (Exp). (b) and (c) Numerical calculation of the transmitted spectra at increasing coupled peak intensity for a pulse centered at 4 μm from *waveguide 2*. In the calculations $n_2 = 5.25 \times 10^{-18}$ m^2/W, $\alpha_{3PA} = 8.8 \times 10^{-28}$ m^3/W^2, $\alpha_{4PA} = 4.76 \times 10^{-41}$ m^5/W^3 (d) The spectral broadening derived from the simulation spectra and from the measurements (Fig. 3(a)) is compared.

#249304 Received 7 Sep 2015; revised 23 Oct 2015; accepted 25 Oct 2015; published 4 Dec 2015

The three- and four-photon absorption coefficients thus estimated are shown in Fig. 5. These values are compared to the ones reported in [22] for similar waveguides probed in the same wavelength range, but using longer, picosecond, pulses. They agree relatively well, considering the error bars. In Fig. 6 the nonlinear refractive index n_2 as a function of wavelength estimated in the experiment is also shown against the results reported in [22] and tends to be slightly higher. We note that in all these experiments, we measure the effective nonlinear parameters for the $Si_{0.6}Ge_{0.4}$/Si waveguides, so that the extracted nonlinear parameters are, strictly speaking, averaged over the waveguide core/cladding geometry rather than being characteristic of the $Si_{0.6}Ge_{0.4}$ core compound alone. Although the mode is mostly confined to the $Si_{0.6}Ge_{0.4}$ core, subtle changes to the geometry could partly explain the differences observed in Fig. 5 and 6 since the measured waveguides, both here and in [22], are somewhat different, and thus having a different distribution of the mode between the Si-Ge core and the Si cladding. Another source of uncertainty in our results is the high sensitivity of the model to different parameters determining the nonlinear response of the waveguide. This increases the error bars of our results as compared to those of [22]. Furthermore, our theoretical model omits some effects that may contribute to the total nonlinear response of the waveguide for femtosecond pulses, such as intra-pulse Raman scattering or self-steepening [25]. Nevertheless, the nonlinear parameters estimated here are close to those estimated in [22], supporting the reliability of the measurements and of our results.

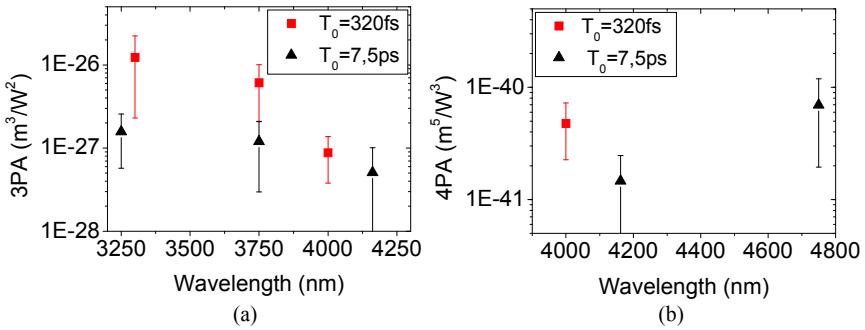

Fig. 5. (a) Three- and (b) four-photon absorption coefficients as a function of wavelength estimated from the transmission measurements using optical pulses with a FWHM duration of 320 fs (this work) and of 7.5 ps [22].

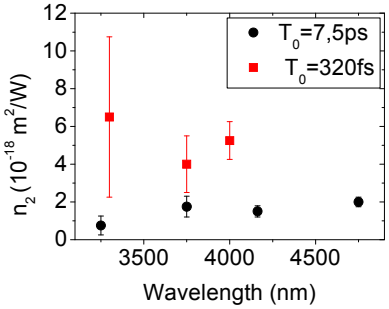

Fig. 6. Nonlinear refractive index as a function of wavelength estimated from the SPM measurements using optical pulses with a FWHM duration of 320 fs (this work) and of 7.5 ps [22].

5. Nonlinear figure of merit

The coefficients reported in Fig. 5 and 6 can be used to infer whether there is a favorable operating wavelength range for nonlinear devices implemented in the Si-Ge platform for the mid-IR. For this purpose, the nonlinear figure of merit (FOM) for three ($FOM_{3PA} = n_2/\alpha_{3PA}\lambda I_0$)

#249304 Received 7 Sep 2015; revised 23 Oct 2015; accepted 25 Oct 2015; published 4 Dec 2015

and four ($FOM_{4PA} = n_2/\alpha_{4PA}\lambda I_0^2$) photon absorption for both the picosecond and femtosecond measurements was evaluated as a function of wavelength in Fig. 7(a) using a coupled peak intensity I_0 of 10 GW/cm^2. Whenever, at the same wavelength, both three and four-photon absorption is present, only the dominant effect was considered (e.g. at $\lambda = 4.16$ μm the four-photon absorption becomes larger than the three-photon absorption when I_0 is larger than 3.6 GW/cm^2). The FOM thus evaluated varies considerably (between 0.5 to 4) in the probed wavelength range with larger values around $\lambda = 4$ μm. Indeed, at wavelengths close to this value, the three-photon absorption coefficient decreases because the photon energy becomes too small to allow this phenomenon, while the photon energy is almost not enough for the four-photon absorption transition.

Since the FOMs defined above vary with the coupled peak intensity, the maximum FOM as a function of the maximum nonlinear phase shift $\Delta\Phi$ achieved after propagation in a waveguide with a an effective length L_{eff}, defined as in [25], of 1cm and neglecting multiphoton absorption (i.e. $\Delta\Phi = \gamma P_0 L_{eff}$, where P_0 is the coupled peak power of the pulse) is shown in Fig. 7(b). We note that by adopting this definition, the nonlinear phase shift $\Delta\Phi$ is actually larger than the one that would be obtained in an experiment using the same coupled peak intensity. Furthermore, we can also observe that since the propagation loss is small and comparable at all the wavelengths used in the experiment and, in the two different waveguides, the effective length of 1 cm considered here corresponds to a physical waveguide length of 1 cm for all the analysed combinations of wavelength and waveguide. It can be seen that the optimum FOM is obtained at different wavelengths, depending on the nonlinear phase shift which in turn depends on the coupled peak intensity. For nonlinear phase shift smaller than 5π, the highest FOM is obtained at $\lambda = 4$ μm whereas the highest FOM is obtained at $\lambda = 3.75$ μm for larger $\Delta\Phi$. The multiphoton absorption as a function of the nonlinear phase shift is shown in Fig. 7(c). This gives an overestimate of the total nonlinear absorption over the waveguide length, since the power decreases upon propagation thus decreasing the multiphoton absorption. The trend observed in this graph supports the variation of the FOM as a function of both wavelength and $\Delta\Phi$ observed in Fig. 7(b). For a nonlinear phase shift smaller than 5π, the multiphoton absorption is smaller at $\lambda = 4$ μm than at $\lambda = 3.75$ μm whereas the opposite holds for $\Delta\Phi > 5\pi$. This behavior can be explained by considering the relative strength of the three and four photon absorption as a function of I_0, which in turn explains the different trends of the curves shown in Figs. 7(b) and 7(c). Since from Eq. (1) the three-photon absorption increases in proportion to I_0^2 and the four-photon absorption increases in proportion to I_0^3, the four-photon absorption (at $\lambda = 4$ μm) can be lower than the three-photon absorption (at $\lambda = 3.75$ μm) at low coupled peak intensities, while the reverse situation can be achieved at high coupled peak intensities.

#249304 Received 7 Sep 2015; revised 23 Oct 2015; accepted 25 Oct 2015; published 4 Dec 2015

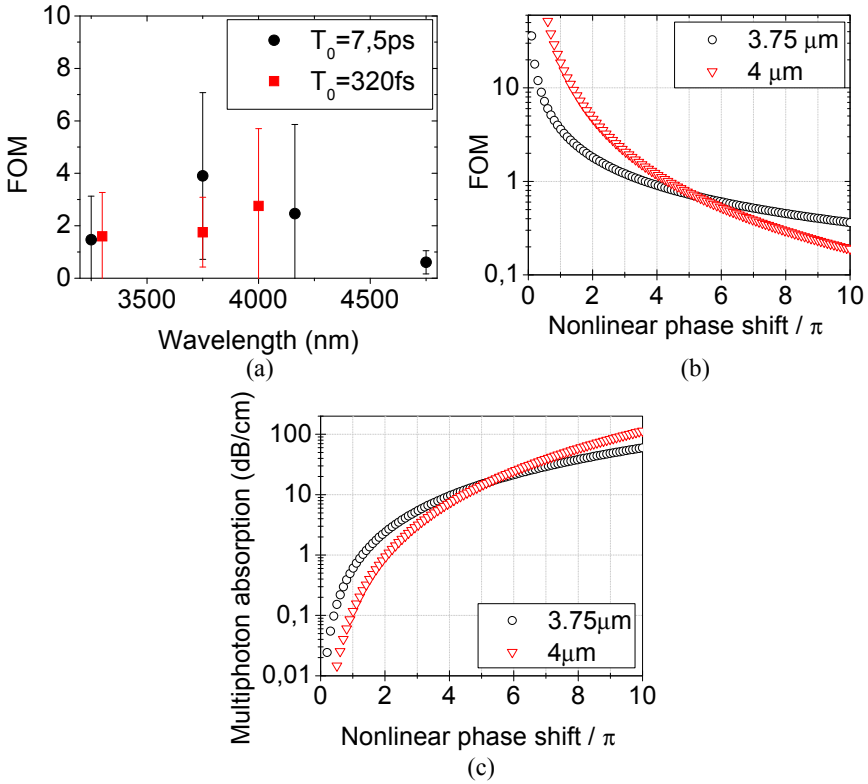

Fig. 7. (a) Nonlinear FOM as a function of wavelength calculated for a coupled peak intensity of 10 GW/cm^2 using the results in Figs. 5 and 6. (b) Nonlinear FOM as a function of nonlinear phase shift $\Delta\Phi = \gamma P_0 L_{eff}$ derived for λ = 3.75μm (circles) and λ = 4μm (triangles) using the results in Figs. 5 and 6. For $\Delta\Phi = \pi$ the coupled peak intensity is 10.7GW/cm^2 at λ = 3.75μm and 3.8GW/cm^2 at λ = 4μm. The wavelength for which the maximum FOM is obtained is 4μm for $\Delta\Phi<5\pi$ and 3.75μm for $\Delta\Phi>5\pi$. (c) Nonlinear losses due to multiphoton absorption as a function of $\Delta\Phi$ derived for λ = 3.75μm (circles) and λ = 4μm (triangles) using the results in Figs. 5 and 6.

Clearly, the analysis presented above is a simplified vision of the impact that nonlinear losses would have on the nonlinear optical response of a device because the free-carrier absorption has been neglected. While free-carrier effects tend to be neglected when using femtosecond pulses in the telecom band, the question is whether or not this is still valid in the mid-IR. In fact, as already pointed out in [18], the FCA increases with the square of the wavelength, thus becoming larger at longer wavelengths. To highlight this point, the ratio between FCA and three-photon absorption (responsible for the free carrier generation in this case) has been calculated. This is given by

$$r = \frac{FCA}{3PA} = \frac{n\sigma E_p}{3\sqrt{3}n_0\hbar\omega_0 A_{5eff}} \tag{3}$$

where n is the Si-Ge refractive index, $\sigma(\lambda) = 1.45 \times 10^{-21} \times (\lambda/1.55)^2$ m^2, n_0 is the effective index of the mode and E_p is the energy of a Gaussian pulse ($E_p = \sqrt{\pi}P_0T_0$ where P_0 is the peak power of the pulse and T_0 is the 1/e pulse duration). From Eq. (3) it can be noted that r does not depend on the three-photon absorption coefficient, but rather, at a fixed wavelength, it depends on the pulse fluence given by E_p/A_{eff}. This is similar to the ratio between TPA and FCA whenever free carriers are generated by TPA [29]. The value of r is plotted as a function

#249304 Received 7 Sep 2015; revised 23 Oct 2015; accepted 25 Oct 2015; published 4 Dec 2015

of the pulse fluence in Fig. 8(a). As it can be seen, the slope increases for longer wavelengths. For example, at the wavelength of 3.3 μm, the effect of FCA becomes dominant over that of three-photon absorption for pulse fluences above 5 mJ/cm^2. This is five times smaller than the threshold between TPA and FCA calculated at 1.55 μm in [29]. In fact, r is roughly proportional to λ^3 since σ is proportional to λ^2 and $\omega_0 = 2\pi c/\lambda$ and thus it is expected to increase rapidly with the wavelength.

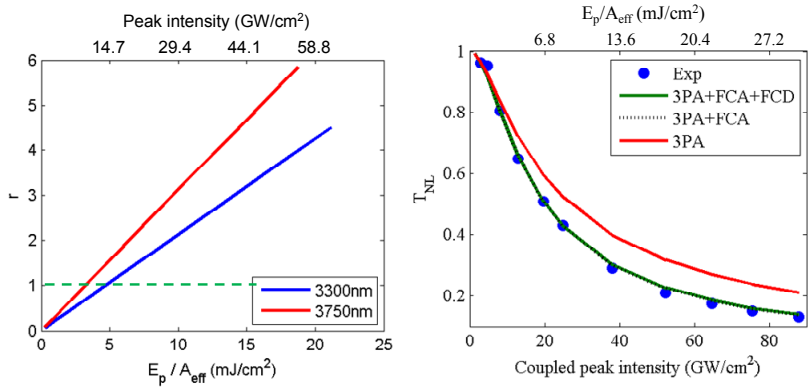

Fig. 8. (a) Ratio r = FCA/3PA as a function of the pulse fluence at a wavelength of 3300 nm and 3750 nm. The dashed green line shows the ordinate r = 1. On the top of the plot the corresponding peak intensity is shown. (b) Normalized transmission as a function of the coupled peak intensity for a 320 fs pulse centered at 3300 nm from *waveguide 1*. The red continuous line is the results when considering only three-photon absorption and neglecting free-carriers effects, for the dotted black line three-photon absorption and FCA are considered and for the continuous green line also free-carrier dispersion (FCD) is considered. On the top of the plot the pulse fluence is shown.

Evidence of the non-negligible impact of FCA in the mid-IR is also found in our simulations. Figure 8(b) shows the normalized transmission as a function of the coupled peak intensity for a 320 fs pulse centered at 3.3 μm. It can be seen that FCA has a non-negligible effect even when using femtosecond pulses and that three-photon absorption alone would not be sufficient to account for the experimental results. This behavior is substantially different from the one observed for femtosecond long optical pulses centered at near-IR wavelengths in Si [27, 29] (where FCA has a negligible effect) and it suggests that, when analyzing the optical nonlinear response of devices in the mid-IR, the effects of free-carriers can create an additional penalty that should be carefully modeled and taken into account.

6. Potential application: Mid-IR supercontinuum

As an illustration of the potential of this material platform, this section is aiming at demonstrating the feasibility of designing efficient mid-IR supercontinuum source based on Si-Ge/Si waveguides and careful dispersion engineering of these waveguides. Figure 9 shows the simulated spectra at various peak intensities for a dispersion engineered waveguide with a cross section of 4 × 2.7 μm^2 and a 500 nm Si top cladding. This is sufficient to get a GVD that is slightly anomalous at wavelengths between 3.8 μm and 6.5 μm (see GVD in Fig. 9(a)). The pump used in these simulations is a 320 fs long pulse centred at 4 μm, corresponding to the wavelength with the highest FOM attainable with this material (see our analysis performed in section V), using pulses with a peak intensity up to 10 GW/cm^2. The A_{eff} used in the calculations is 9.37 μm^2.

#249304 Received 7 Sep 2015; revised 23 Oct 2015; accepted 25 Oct 2015; published 4 Dec 2015

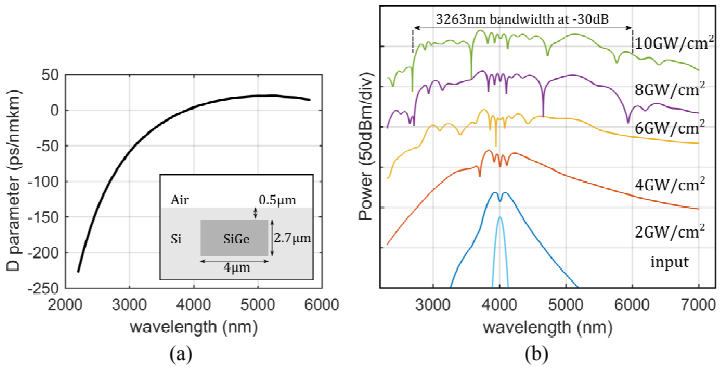

Fig. 9. (a) GVD of the dispersion engineered SiGe waveguide under consideration (in inset) (b) The evolution of the spectrum as a function of the coupled peak intensity into the waveguide as obtained from numerical modelling.

For the simulations, we used Eq. (1) in which we added the third and fourth-order dispersion terms (β_3, β_4). We considered a 6 cm long waveguide with propagation losses of 1 dB/cm and experimental nonlinear values collected and presented in this paper for $Si_{0.6}Ge_{0.4}$/Si step index core waveguide. The calculated transmitted spectra are shown in Fig. 9(b). We can observe that at low peak intensity the spectral broadening is characteristic of SPM. As the power increases a −30 dB witdh supercontinuum spanning the entire 2.5 to 6 μm range (i.e. more than an octave spanning) is generated. These calculations clearly show that multiphoton absorption and the effects of the photo-generated free-carrier in the mid-IR using Si-Ge/Si waveguides will not preclude applications for which a strong nonlinear response is required such as supercontinuum generation.

7. Conclusion

We report measurements of the nonlinear optical response of low-loss $Si_{0.6}Ge_{0.4}$/Si waveguides in the mid-IR between 3.3 μm and 4 μm using femtosecond long pulses. In this wavelength range, nonlinear losses due to multi-photon absorption and the associated generation of free-carriers were observed at high peak intensities. We estimate the three- and four-photon absorption coefficients together with the nonlinear refractive index of $Si_{0.6}Ge_{0.4}$/Si waveguides, which are found to be comparable to previous work [22] on the same material but with different waveguide length and geometries, and with longer optical pulses. Therefore, this work corroborates the previous measurements and thus provides some guidelines for future nonlinear device work. Using the estimated coefficients, the nonlinear FOM of $Si_{0.6}Ge_{0.4}$/Si waveguides in the mid-IR is evaluated. An optimum FOM is observed around 4 μm due to the decrease of the three-photon absorption coefficient, together with a small four-photon absorption coefficient. We find that this optimum of the FOM also depends on the coupled peak intensity since the three and four-photon absorption scales differently with this parameter. Furthermore, we observe that the impact of free-carriers is significant even though the pulse duration is only a few hundreds of femtoseconds. This is in contrast with what is usually observed at near-IR wavelengths, and highlights the need to accurately account for free-carrier effects even when using ultra-short optical pulses in the mid-IR. These results, together with [22], represent the first experimental characterization of the nonlinear optical response of $Si_{0.6}Ge_{0.4}$/Si waveguides in the mid-IR. This work provides useful groundwork for the design of photonic devices such as supercontinuum sources based on this material platform and will go a long way towards the understanding of the optical nonlinear response of this material system in the mid-IR wavelength range.

#249304 Received 7 Sep 2015; revised 23 Oct 2015; accepted 25 Oct 2015; published 4 Dec 2015

Acknowledgment

This work was supported by the People Program (Marie Curie Actions) of the European Union's Seventh Framework Program FP7/2007-2013 under REA grant agreements n° PCI-GA-2013-631543 and n° PCIG10-GA-2011-304005, the French National Research Agency (ANR project MOREMIR), the Institut Universitaire de France and was conducted within the context of the International Associated Laboratory "ALPhFA: Associated Laboratory for Photonics between France and Australia". This research was in part supported by the Australian Research Council Centre of Excellence for Ultrahigh bandwidth Devices for Optical Systems (project number CE110001018).

#249304 Received 7 Sep 2015; revised 23 Oct 2015; accepted 25 Oct 2015; published 4 Dec 2015